

# Heteroanionic Stabilization of Ni<sup>1+</sup> with Nonplanar Coordination in Layered Nickelates

Jaye K. Harada,<sup>1</sup> Nenan Charles,<sup>1</sup> Nathan Z. Koocher,<sup>1</sup> Yiran Wang,<sup>2</sup>  
Kenneth R. Poeppelmeier,<sup>2</sup> Danilo Puggioni,<sup>1,\*</sup> and James M. Rondinelli<sup>1,†</sup>

<sup>1</sup>*Department of Materials Science and Engineering,  
Northwestern University, Evanston, Illinois, 60208, USA*

<sup>2</sup>*Department of Chemistry, Northwestern University, Evanston, Illinois 60208, USA*

(Dated: April 18, 2023)

We present electronic structure calculations on layered nickelate oxyfluorides derived from the Ruddlesden-Popper arisotype structure in search of unidentified materials that may host nickelate superconductivity. By performing anion exchange of oxygen with fluorine, we create two heteroanionic La<sub>2</sub>NiO<sub>3</sub>F polymorphs and stabilize Ni<sup>1+</sup> in 4-coordinate and 5-coordinate square planar and square pyramidal geometries, respectively. We further predict chemical reactions with high thermodynamic driving forces to guide their synthesis. These oxyfluorides are weakly correlated antiferromagnetic insulators and their nonmagnetic phases exhibit quasi-2D Fermi surfaces dominated by Ni  $d_{x^2-y^2}$  states, which strikingly resemble undoped cuprate superconductors. We discuss how the oxyfluoride anion chemistry promotes Ni-O covalency and single-band character that is more similar to the cuprates than homoanionic infinite-layer nickelates. We use our understanding to propose doping strategies and layered LaSrNiO<sub>2</sub>F<sub>2</sub> and La<sub>3</sub>Ni<sub>2</sub>O<sub>4</sub>F<sub>3</sub> nickelate oxyfluorides with tunable electronic and magnetic structures for experimentation.

The electronic structure of complex transition metal compounds can be designed to exhibit a myriad of correlated physics and functional phenomena [1–6]. RNiO<sub>3</sub> nickelates are an exemplary family with this tunability [7]. They exhibit metal-to-insulator, paramagnetic-to-antiferromagnetic, and bond/charge-ordering transitions with critical temperatures governed by choice of the rare earth  $R$  cation [8–10], which inductively modifies the Ni  $d$ - $p$  orbital interactions [11]. Further tailoring may be obtained with epitaxial strain, heterostructuring, or light to modulate and even suppress these transitions [12]. More recently, the electronic-orbital dependencies on the Ni cation coordination has been exploited in search of novel nickelate superconductors. The guiding discovery approach has been to mimic the electronic structure of superconducting cuprate oxides and oxyhalides, where Cu exhibits planar or square pyramidal coordination [13–15], by modifying the atomic scale structure to control the orbital occupations [16–21]. Most attempts in 3D nickelates have led to minimal orbital polarizations and the absence of superconductivity.

Nickelate superconductivity remained unsuccessful until the recent synthesis of two-dimensional (2D) thin films of Sr-doped NdNiO<sub>2</sub> and PrNiO<sub>2</sub> [22–28]. These were obtained through a process of thin-film deposition followed by soft-chemistry methods [29], utilizing a strong topotactic metal hydride reduction reaction that simultaneously achieves both a planar 2D atomic structure and electrochemically drives Ni into the difficult to obtain +1 oxidation state [16] with a formal  $t_{2g}^6 e_g^3$  ( $S = 1/2$ ) electronic configuration matching Cu<sup>2+</sup> in the isostructural infinite-layer cuprate CaCuO<sub>2</sub>. Nonetheless, the observed maximum superconducting critical temperature ( $T_c \sim 15$  K) is well below that of high- $T_c$  cuprates ( $T_c \sim 133$  K) [30], and

the nickelate transport properties strongly depend on sample quality [22, 31, 32]. This sensitivity likely arises from the aggressive reduction reaction, which although creating and replicating the 2D cuprate topology, also leads to unintentional hydride incorporation to form a mixed-anion nickelate oxyhydride with heteroleptic NiO<sub>4</sub>H<sub>2</sub> octahedra [33]. These findings suggest H is an important ingredient to both realizing the 2D structure and superconductivity—the materials may be better described as heteroanionic infinite-layer nickelates comprising more than one anion.

Here we propose the intentional creation of heteroanionic nickelates as an alternative strategy to realize analogous cuprate physics, and as we emphasize below, essential materials chemistry, by starting from quasi-2D bulk oxides and exploiting multi-anion rather than cation effects [34–37]. Consider the  $R_{n+1}Ni_nO_{3n+1}$  Ruddlesden-Popper (RP) structure, which exhibits alternating  $n$  perovskite planes of corner-connected NiO<sub>6</sub> octahedra interleaved between rock-salt  $RO$  sheets. The ideal  $n = 1$  RP oxide with the K<sub>2</sub>NiF<sub>4</sub>- or T-type structure (space group  $I4/mmm$ ) hosts Ni<sup>2+</sup> ( $t_{2g}^6 e_g^2$ ,  $S = 1$ ) and is distinct from other layered nickelates [38, 39]. It may be written as  $(R^{3+})_2 \infty [\text{NiO}_{4'/2'}\text{O}_{2/1}]^{6-}$  [40], revealing that there are infinite layers of octahedra comprising 4 linear-bridging and 2 terminal oxide anions (Fig. 1a). Since fluorine prefers to occupy terminal sites in RP oxyfluorides [41], equal exchange of oxygen with the lower valence fluoride anion reduces the metal to Ni<sup>1+</sup> while splitting the apical sites:  $(R^{3+})_2 \infty [\text{NiO}_{4'/2'}\text{O}_{1/1}\text{F}_{1/1}]^{6-} = R_2\text{NiO}_3\text{F}$ . Hence, the square-planar geometric requirement proposed by Anisimov [16], and pursued over the last three decades of nickelate research to stabilize Ni<sup>1+</sup>, can be inherently circumvented in oxyfluorides. Yet, there remains ambiguity in whether the octahedral geometry persists or transforms

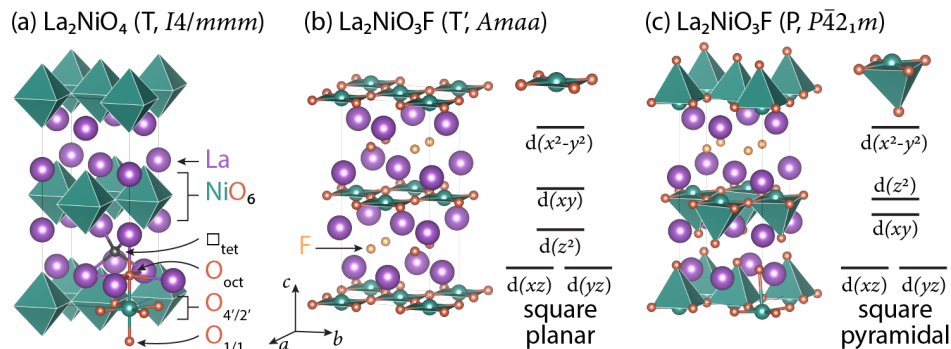


FIG. 1. (a) Aristotype Ruddlesden-Popper  $\text{La}_2\text{NiO}_4$  oxide nickelate with the T-type structure and derived  $\text{La}_2\text{NiO}_3\text{F}$  polymorphs with the (b) T' structure and (c) P structure. The corresponding representative crystal field splitting energy levels are shown for both the square planar and square pyramidal Ni coordination geometries.

to square planar or square pyramidal coordination, and in doing so, which sites the displaced ligands occupy.

We examine with density functional theory (DFT) the variety of structure types and local environments that RP-derived oxyfluoride nickelates adopt in search of candidate bulk heteroanionic nickelate superconductors. We create two polymorphs differing by their local Ni coordination environment and position of the fluoride anions relative to the oxygen anions. The first phase of  $\text{La}_2\text{NiO}_3\text{F}$  exhibits square-planar coordinated Ni cations (Fig. 1b), and we refer to it as T' following the convention for this hettotype (Table S1 of the Supporting Information [42]). The structure is obtained from a  $\sqrt{2} \times \sqrt{2} \times 1$  transformation of the RP  $I4/mmm$  structure with ordered terminal anion vacancies, i.e.,  $(\text{La})_2 \overset{2}{\infty} [\text{NiO}_{4'/2'} \square_{2/1}]$ . Then, interstitial tetrahedral sites in the (001) plane between the La cations are decorated with [100] anion stripes that alternate between O and F along [010] to produce  $(\text{La}_2\text{O}_{4''/4}\text{F}_{4''/4}) \overset{2}{\infty} [\text{NiO}_{4'/2'}]$  or the  $\text{La}_2\text{NiO}_3\text{F}$  stoichiometry [43]. Adjacent planes of these interstitial anions are translated relative to each other by  $1/2b$ . We then performed a full relaxation of the structure with DFT [42], and found that the equilibrium geometry exhibits antipolar La displacements along the [110] direction which reduces the crystal symmetry to orthorhombic  $Amaa$ . Previously, a tetragonal structure with a different O-F arrangement and  $I\bar{4}m2$  symmetry was studied [36]; however, the calculated energy difference between the  $I\bar{4}m2$  and  $Amaa$  phases is  $\sim 100$  meV/f.u. favoring the latter as more stable.

Next, we examined  $\text{La}_2\text{NiO}_3\text{F}$  with square-pyramidal Ni coordination, which we refer to as the P structure (Table S1). It is a derivative of the ordered  $n = 1$  RP heteroanionic oxyfluoride  $\text{Sr}_2\text{FeO}_3\text{F}$  (space group  $P4/nmm$ ) [44]. In contrast to the T-type structure,  $\text{Sr}_2\text{FeO}_3\text{F}$  exhibits *trans* ordering of the terminal O/F anions at the apical octahedral sites. This results in a strong distortion of the  $\overset{2}{\infty} [\text{FeO}_{4'/2'}\text{O}_{1/1}\text{F}_{1/1}]$ . The F anion significantly displaces away from Fe along the *trans* bond into the

Sr layers but it does not occupy the tetrahedral interstitial site, i.e.,  $(\text{Sr}_2\text{F}_{1/1}) \overset{2}{\infty} [\text{FeO}_{4'/2'}\text{O}_{1/1}]$ . We fully relaxed this structure and several distorted variants of this derivative and found that unlike  $\text{Sr}_2\text{FeO}_3\text{F}$ , the fluoride ions always move from the octahedral (oct) to tetrahedral (tet) interstitial site to form  $\text{NiO}_5$  square pyramidal polyhedra (Fig. 1c). In both T' and P polymorphs the fluorine ions prefer to occupy the interstitial tetrahedral sites (Fig. 1b,c). The lowest energy P structure is non-centrosymmetric with tetragonal  $P\bar{4}2_1m$  symmetry and exhibits alternating  $a^-b^0c^0$  and  $a^0b^-c^0$  Glazer tilts [45] in adjacent layers along the [001] direction. In layered cuprate superconductors, the copper-apical-oxygen distance ( $\text{Cu}-\text{O}_{ap}$ ) correlates with the maximal  $T_c$  [46–48]; in the P structure, the Ni- $\text{O}_{ap}$  distance is 2.62 Å, which is intermediate between  $\text{YBa}_2\text{Cu}_3\text{O}_{6.9}$  ( $\sim 2.28$  Å [49]) and  $\text{HgBa}_2\text{CuO}_6$  ( $\sim 2.80$  Å [50]).

We further confirmed the dynamical stability of both phases (Fig. S1). Although both polymorphs are dynamically stable, the P structure is  $\approx 570$  meV higher in energy than the T' phase. Recent synthesis of  $\text{La}_2\text{NiO}_3\text{F}$  and  $\text{Pr}_2\text{NiO}_3\text{F}$  using solid-solid reactions with topochemical hydride-based defluorination supports this finding, which reported structures with square planar  $\text{NiO}_4$  [43, 51]. Magnetic measurements on these oxyfluoride powders found spin-glass behavior similar to the infinite layer oxide nickelates, while DFT calculations predict a strongly antiferromagnetic phase [36]. Such discrepancies may arise from inhomogeneity in the fluoride concentration, which causes variability in the local Ni coordination, valence, and overall hole concentration.

These complexities may be overcome by identifying a synthetic reaction that provides a high thermodynamic driving force for phase formation [52]. To that end, we calculate the reaction chemical potentials ( $\Delta\mu_{\text{rxn}}$ ) for several solid-solid, solid-liquid, and solid-gas reactions to assess which provides the highest driving force for the P structure (Table S2). The solid-state reaction, i.e.,  $\text{LaNiO}_2 + \text{LaOF} \rightarrow \text{La}_2\text{NiO}_3\text{F}$ , which does not change the

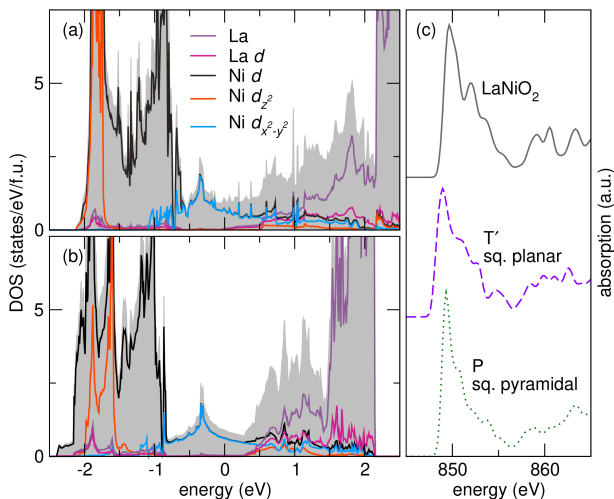
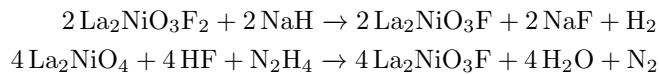


FIG. 2. Projected density of states (DOS) of  $\text{La}_2\text{NiO}_3\text{F}$  with the (a)  $T'$  and (b) P structures with  $E_F = 0$  eV. (c) Simulated Ni L-edge XAS spectra of relevant nickelates.

Ni oxidation state, does not provide a sufficient driving force for either the P or lower-energy  $T'$  phases ( $\Delta\mu_{\text{rxn}} = 0.82$  eV/f.u. and  $0.24$  eV/f.u., respectively). Thus, we pursued distinct Ni redox pathways and found that the most promising reactions to produce the P polymorph were a solid-solid reaction with sodium hydride and a reaction with hydrazine in aqueous HF(aq):



with  $\Delta\mu_{\text{rxn}} = -1.09$  eV/f.u. and  $-0.33$  eV/f.u., respectively. Because hydrothermal reactions can produce metastable phases and have tunable pH, temperature, and ion concentrations, which enable high polymorphic selectivity of heteroanionic oxyfluoride and oxychalcogenide products [53, 54], we believe this is a viable route to produce the P structure. Phase purity of it can be ascertained both with X-ray diffraction and second harmonic generation measurements.

Next, we examine the projected density of states (DOS) for the nonmagnetic phases of both the  $T'$  and P polymorphs (Fig. 2a,b). Fig. S2 shows the DOS over a wider energy range with more orbital projections. Both nonmagnetic phases are metals and the Fermi level ( $E_F$ ) is dominated by the Ni  $3d_{x^2-y^2}$  states. The La  $5d$  states located nearby at higher energy [36], and they self-dope the  $T'$  phase as in homoanionic nickelates but are fully empty in the P phase. Owing to the different Ni coordination environments, the Ni  $3d$  orbitals crystal field splitting energy diagrams are distinct (Fig. 1). This is clearly seen through the position of the  $3d_{z^2}$  orbital, which comprises the bottom of the nominal Ni  $3d$ -derived valence band around  $\sim -1.9$  eV in the  $T'$  structure compared to the P structure at  $\sim -1.7$  eV. The O and F  $2p$  states are separated from the Ni  $3d$  states by a  $\sim 1$  eV electronic

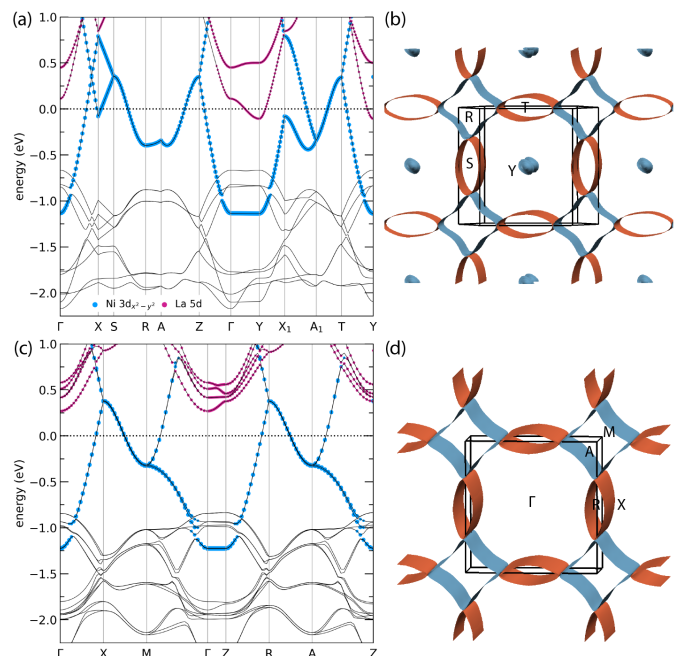


FIG. 3. Band structures (a,c) and Fermi surfaces (b,d) of  $T'$  and P  $\text{La}_2\text{NiO}_3\text{F}$  polymorphs, respectively. Both Fermi surfaces exhibit electron (light blue) and hole (orange) pockets.

band gap (Fig. S3). First, the F  $2p$  states are located below  $\sim -6$  eV and exhibit a different degree of localization in the two phases. Those states are more localized in the  $T'$  crystal structure. This is due to the 1D striped arrangement of the F anions in the structure in contrast to the 2D net in the P structure. Second, the O  $2p$  states fall into two separate energy windows: approximately  $[-8.2, -3.2]$  and  $[-2, -0.6]$  eV for the  $T'$  phase and  $[-8.8, -3.5]$  and  $[-2.1, -0.9]$  eV for the P phase (Fig. S2 and Fig. S3). This distribution alters the O( $2p$ )-Ni( $3d$ ) hybridization and has a profound effect on covalency (infra vide).

Our analysis of both  $\text{La}_2\text{NiO}_3\text{F}$  polymorphs suggests that Ni is in the  $1+$  oxidation state ( $3d^9$ ) and is isoelectronic to  $\text{Cu}^{2+}$ . To assess the oxidation state, we computed the Ni L-edge X-ray absorption spectrum (XAS) [42]. Fig. 2c shows the simulated spectra for  $T'$  and P  $\text{La}_2\text{NiO}_3\text{F}$  and the infinite-layer nickelate  $\text{LaNiO}_2$ . All simulated spectra occur at the similar energy, starting at approximately 846 eV, suggesting that each compound comprises Ni cations with the same valence. The line-shapes of the spectra are also similar. Our calculated  $\text{LaNiO}_2$  spectrum exhibits two peaks in a 2 eV range from  $\sim 850$  to  $\sim 852$  eV. Both the  $T'$  and P structures have two peaks in this range such that the low-energy L-edge spectra are similar to  $\text{LaNiO}_2$ . Next, we validate our calculated  $\text{LaNiO}_2$  spectra by comparing to experiment upon aligning the first peak of each spectra [55]. The experimental spectrum of  $\text{LaNiO}_2$  shows two peaks in about a 2 eV range [56], approximately from 852 to 854 eV, which is similar to the two peaks obtained in a 2 eV peak range

from our model. This agreement supports the assignment of  $\text{Ni}^{1+}$  in two distinct coordination environments.

Fig. 3a,b shows the nonspin-polarized band structure and Fermi surface for  $T'$   $\text{La}_2\text{NiO}_3\text{F}$ . The only bands crossing  $E_F$  originate from the Ni  $3d_{x^2-y^2}$  and La  $5d_{z^2}$  orbitals. Moving along the  $S$ - $Z$  and  $A_1$ - $T$  directions, the Ni  $3d_{x^2-y^2}$  band is doubly degenerate. Then it splits and forms two single degenerate bonding and antibonding bands along the  $\Gamma$ - $S$ ,  $Z$ - $A_1$ , and  $T$ - $Y$  trajectories. The Fermi surface is quasi-2D and composed of two hole pockets at  $S$  and  $T$  and one electron pocket at  $R$  with Ni  $3d_{x^2-y^2}$  character. Moreover, there is an electron knob at  $Y$  from the La  $5d_{z^2}$  band. The corresponding electronic structures for the P structure are shown in Fig. 3c,d. As in the  $T'$  structure, the highly dispersive Ni  $3d_{x^2-y^2}$  band exhibits 2D character and produces a Fermi surface with hole and electron pockets centered around the  $X$  and  $M$  points of the Brillouin zone, respectively. The major electronic difference between the square pyramidal P structure and the square planar  $T'$  structure is that the position of the La  $5d_{z^2}$  band is well above the  $\Gamma$  point ( $\sim 0.25$  eV) and does not cut  $E_F$  in the P structure (cf. Fig. 3a,c).

Interestingly, both Fermi surfaces exhibit reduced  $O(2p)$ -Ni( $3d$ ) hybridization as the oxygen states are shifted to lower energy and more strongly mix with orbitals without  $d_{x^2-y^2}$  character. This is in contrast to that found in the high- $T_c$  cuprates where Zhang-Rice singlets and orbital symmetry are important [26, 36, 57, 58]. Furthermore, our computed Fermi surfaces are distinct from those of the infinite-layer nickelate  $\text{LaNiO}_2$  [26] and a nickelate oxyfluoride phase studied in Ref. 36. Apart from the different space group (Brillouin zone) and lattice periodicity (band folding), we find nested electron and hole pockets with Ni  $3d_{x^2-y^2}$  character touch each other. This suggests that, in both polymorphs, the Ni band  $3d_{x^2-y^2}$  is exactly half-filled, as expected in an undoped scenario where the oxidation state of Ni is exactly  $1+$ .

We also find that both  $T'$  and P polymorphs exhibit G-type antiferromagnetic (AFM) order with antiferromagnetic (001) in-plane nearest-neighbor Ni superexchange. The G-type magnetic ordering is 38 meV and 23 meV lower in energy than the nonmagnetic model for the  $T'$  and P structures, respectively. The computed local magnetic moments are  $\sim 0.60 \mu_B$  for both polymorphs, further confirming  $\text{Ni}^{1+}$ . We further modeled the exchange interactions for  $\text{Ni}^{1+}$  ( $S = 1/2$ ) using a Heisenberg spin Hamiltonian to obtain the in-plane exchange  $J_{in} = -38$  meV and  $-23$  meV for the  $T'$  and P structures [42], respectively. The AFM in-plane exchange of  $\text{La}_2\text{NiO}_3\text{F}$  is strongly reduced compared to that of cuprate compounds such as  $\text{La}_2\text{CuO}_4$  and  $\text{CaCuO}_2$  ( $J = 120$  meV) [59].

Both magnetically ordered AFM-G  $T'$  and P polymorphs are insulating (Fig. 4a,b) with DFT electronic band gaps of  $E_g = 150$  meV and 300 meV, respectively, which makes them Slater insulators and conducive to ambipolar doping [42]. Undoped cuprates are described

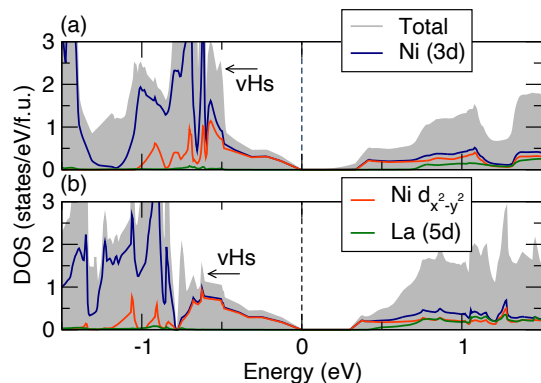


FIG. 4. The projected density of states (DOS) of the AFM G-type (a)  $T'$  and (b) P polymorphs of  $\text{La}_2\text{NiO}_3\text{F}$ . A shift of the Fermi level to the van Hove singularities (vHs), indicated by the arrows, corresponds to doping of 0.25 hole/f.u. and 0.33 hole/f.u. for the  $T'$  and P phases, respectively.

as AFM Mott insulators [60] and the van Hove singularities (vHs) in their electronic structure are used to estimate optimal doping for maximizing  $T_c$  [61]. In the DOS shown in Fig. 4, the vHs are located at 0.51 eV and 0.62 eV below  $E_F$ , which gives optimal dopings at 0.25 hole/f.u. and 0.33 hole/f.u. for the  $T'$  and P polymorphs, respectively, where minima in the Seebeck coefficients are also expected as in cuprates [62]. Although these hole concentrations are higher than reported for cuprates ( $\sim 0.16$  hole/f.u.) [63] and layered square-planar nickelate oxides ( $\sim 0.2$  hole/f.u.) [39], they should be readily accessible through cation substitution, e.g., alkaline-earth metals, or through anion insertion with excess oxygen onto unoccupied interstitial sites.

We also examined the electronic structures of two other  $\text{Ni}^{1+}$  oxyfluorides with O:F anion ratios:  $\text{LaSrNiO}_2\text{F}_2$  and  $\text{La}_3\text{Ni}_2\text{O}_4\text{F}_3$ , which have square planar  $[\text{NiO}_{4/2'}]^{7-}$  and square pyramidal  $[\text{NiO}_{4/2'}\text{F}_{1/1}]^{8-}$  coordinations, respectively (Table S3). They are also narrow gap AFM Slater insulators [42]. All oxyfluorides examined exhibit 2D electronic structures like that recently predicted for infinite-layer nickelates with hydrogen incorporation [64], where  $\text{H}^-$  anions were found to occupy apical Ni coordination sites, because the absence of  $\pi$  symmetry in the hydride  $1s$  orbital makes it a chemical “scissor” that blocks interlayer electron hopping. In contrast, the 2D Fermiology of the oxyfluorides and hole dopability is due to the distance between the  $\text{NiO}_4$  plane, which is  $c/2$  ( $< c/2$ ) in the  $T'$  (P) structure, and the LaO layers. The interlayer distance is large because it is enhanced by interstitial F occupation. These oxyfluoride crystal chemistry principles may be used in the same manner as employed by Goodenough and Manthiram to understand how interlayer stresses control electronic compensation and superconductivity in layered cuprates [65].

The covalency and bond anisotropy in cuprates is fun-

damental to their large superexchange strengths and high  $T_c$  [66]. The RP-derived oxyfluorides possess this added feature of exhibiting more overall covalent character (less ionicity) compared to the homonanionic layered nickelate oxides. Despite the addition of more electronegative  $F^-$ , which reduces the in-plane AFM exchange, the fluoride states at lower energy constrain and shift the active oxygen band centers closer to the  $d$  orbitals. The reduced energy separation, created through an inductive effective [67], strengthens the formation of the low energy antibonding  $d$ -orbital derived states (Fig. S3). We find the oxyfluorides are more covalent than the prototype  $\text{LaNiO}_2$  owing to increased  $O(2p)$ - $Ni(3d)$  overlap at the expense of reduced orbital bandwidth from the multi-anion effect. The response is analogous to interlayer charge transfer found in layered cuprates mediated by oxygen displacements [68], where out-of-plane electron transfer increases the in-plane ligand hole density [69]. We quantify this effect in terms of percentage ionicity [70]. The ionicities of the nickelate oxyfluorides are similar and closer to the cuprates than the homonanionic nickelates: 49.1% for  $\text{La}_2\text{NiO}_3\text{F}$ , 51.2% for  $\text{LaSrNiO}_2\text{F}_2$ , and 48.8% for  $\text{La}_3\text{Ni}_2\text{O}_4\text{F}_3$  versus the undoped superconductors YBCO,  $\text{CaCuO}_2$ , and  $\text{LaNiO}_2$  with ionicities of 49.4%, 52.0%, and 57.0%, respectively. Additional similarities and differences are in Table S4.

In summary, we investigated the structural, electronic and magnetic properties of several  $\text{Ni}^{1+}$  oxyfluorides and showed that they have more similarities to cuprates than the infinite layer nickelate oxides. As undoped compounds, they are weakly correlated antiferromagnetic insulators exhibiting near or complete isolation of the  $d_{x^2-y^2}$  orbital enabled by  $F^-$ . In  $T'$   $\text{La}_2\text{NiO}_3\text{F}$ , we found the  $R$ -derived  $5d$  state is near the Fermi level, as in other (hydrogen incorporated) infinite layer nickelates, but that state is absent in the P polymorph. This makes oxyfluorides an attractive platform to discern contributions from multi-band physics to the superconductivity mechanism and whether those states limit access to higher temperature scales. We further identified that bond covalency may be an essential component neglected in prior searches. This finding should be interpreted through more detailed studies of electron correlation effects to better understanding the role played by spin fluctuations at finite temperatures. Incorporating doping of nickelate oxyfluorides using hydrothermal reactions and/or topotactic fluorination of thin films, which have been shown to produce metastable phases and compliments current thin-film approaches based on heteroepitaxy or superlattice formation [71, 72], are needed. Given that oxyfluorides adopt a wide variety of structure types, including some that are unique from complex oxides [73–76], we conjecture there are several unidentified superconducting nickelate oxyfluoride candidates to be found. Similarly, nickel oxyhalides with  $\text{Cl}^-$  or  $\text{Br}^-$  are other exciting materials families.

Electronic structure studies were supported by the National Science Foundation (NSF) through award DMR-

2011208 while the synthesis science efforts were supported by the NSF’s MRSEC program (DMR-1720319) at the Materials Research Center of Northwestern University. Calculations were performed using the Department of Defense High Performance Computing Modernization Program (DOD-HPCMP) and the Carbon cluster at the Center for Nanoscale Materials, a U.S. Department of Energy Office of Science User Facility, supported by the U.S. DOE, Office of Basic Energy Sciences, under Contract No. DE-AC02-06CH11357.

---

\* [daniло.puggioni@northwestern.edu](mailto:daniло.puggioni@northwestern.edu)

† [jrondinelli@northwestern.edu](mailto:jrondinelli@northwestern.edu)

- [1] J. Zhang, L. Song, G. K. H. Madsen, K. F. F. Fischer, W. Zhang, X. Shi, and B. B. Iversen, Designing high-performance layered thermoelectric materials through orbital engineering, *Nature Communications* **7**, 10892 (2016).
- [2] M. K. Wu, J. R. Ashburn, C. J. Torng, P. H. Hor, R. L. Meng, L. Gao, Z. J. Huang, Y. Q. Wang, and C. W. Chu, Superconductivity at 93 K in a new mixed-phase Y-Ba-Cu-O compound system at ambient pressure, *Physical Review Letters* **58**, 908 (1987).
- [3] M. Kargarian and G. A. Fiete, Topological crystalline insulators in transition metal oxides, *Phys. Rev. Lett.* **110**, 156403 (2013).
- [4] J. Bockris and T. Otagawa, The electrocatalysis of oxygen evolution on perovskites, *J. Electrochem. Soc.* **131**, 290 (1984).
- [5] M. Imada, A. Fujimori, and Y. Tokura, Metal-insulator transitions, *Reviews of Modern Physics* **70**, 1039 (1998).
- [6] H. Ohta, K. Sugiura, and K. Koumoto, Recent Progress in Oxide Thermoelectric Materials:  $p$ -Type  $\text{Ca}_3\text{Co}_4\text{O}_9$  and  $n$ -Type  $\text{SrTiO}_3$ , *Inorganic Chemistry* **47**, 8429 (2008), pMID: 18821809.
- [7] Z. Zhang, Y. Sun, and H.-T. Zhang, Quantum nickelate platform for future multidisciplinary research, *Journal of Applied Physics* **131**, 120901 (2022).
- [8] J. Chaloupka and G. Khaliullin, Orbital Order and Possible Superconductivity in  $\text{LaNiO}_3/\text{LaMO}_3$  Superlattices, *Physical Review Letters* **100**, 016404 (2008).
- [9] J. Varignon, M. N. Grisolia, J. Iniguez, A. Barthélemy, and M. Bibes, Complete phase diagram of rare-earth nickelates from first-principles, *npj Quantum Materials* **2**, 1 (2017).
- [10] S. Middey, J. Chakhalian, P. Mahadevan, J. Freeland, A. Millis, and D. Sarma, Physics of ultrathin films and heterostructures of rare-earth nickelates, *Annual Review of Materials Research* **46**, 305 (2016).
- [11] J.-G. Cheng, J.-S. Zhou, J. B. Goodenough, J. A. Alonso, and M. J. Martinez-Lope, Pressure dependence of metal-insulator transition in perovskites  $R\text{NiO}_3$  ( $R = \text{Eu}, \text{Y}, \text{Lu}$ ), *Phys. Rev. B* **82**, 085107 (2010).
- [12] V. A. Stoica, D. Puggioni, J. Zhang, R. Singla, G. L. Dakovski, G. Coslovich, M. H. Seaberg, M. Kareev, S. Middey, P. Kissin, R. D. Averitt, J. Chakhalian, H. Wen, J. M. Rondinelli, and J. W. Freeland, Magnetic order driven ultrafast phase transition in  $\text{NdNiO}_3$ , *Phys. Rev. B* **106**, 165104 (2022).

- [13] J. Karpinski, H. Schwer, I. Mangelschots, K. Conder, A. Morawski, T. Lada, and A. Paszewin, Single crystals of  $\text{Hg}_{1-x}\text{Pb}_x\text{Ba}_2\text{Ca}_{n-1}\text{Cu}_n\text{O}_{2n+2+\delta}$  and infinite-layer  $\text{CaCuO}_2$ . synthesis at gas pressure 10 kbar, properties and structure, *Physica C: Superconductivity* **234**, 10 (1994).
- [14] S. Banerjee, C. Dasgupta, S. Mukerjee, T. V. Ramakrishnan, and K. Sarkar, High temperature superconductivity in the cuprates: Materials, phenomena and a mechanism, *AIP Conference Proceedings* **2005**, 020001 (2018), <https://aip.scitation.org/doi/pdf/10.1063/1.5050718>.
- [15] H. Ninomiya, K. Kawashima, A. Iyo, H. Fujihisa, S. Ishida, H. Ogino, Y. Yoshida, Y. Gotoh, and H. Eisaki, Calcium-free double-layered cuprate superconductors with critical temperature above 100 K, *Commun. Mater.* **2**, 13 (1994).
- [16] V. I. Anisimov, D. Bukhvalov, and T. M. Rice, Electronic structure of possible nickelate analogs to the cuprates, *Physical Review B* **59**, 7901 (1999).
- [17] P. Hansmann, A. Toschi, X. Yang, O. K. Andersen, and K. Held, Electronic structure of nickelates: From two-dimensional heterostructures to three-dimensional bulk materials, *Phys. Rev. B* **82**, 235123 (2010).
- [18] M. J. Han, C. A. Marianetti, and A. J. Millis, Chemical control of orbital polarization in artificially structured transition-metal oxides:  $\text{La}_2\text{NiXO}_6$  ( $X = \text{B}, \text{Al}, \text{Ga}, \text{In}$ ) from first principles, *Phys. Rev. B* **82**, 134408 (2010).
- [19] V. V. Poltavets, M. Greenblatt, G. H. Fecher, and C. Felser, Electronic Properties, Band Structure, and Fermi Surface Instabilities of  $\text{Ni}^{1+}/\text{Ni}^{2+}$  Nickelate  $\text{La}_3\text{Ni}_2\text{O}_6$ , Isoelectronic with Superconducting Cuprates, *Phys. Rev. Lett.* **102**, 046405 (2009).
- [20] H. Chen, D. P. Kumah, A. S. Disa, F. J. Walker, C. H. Ahn, and S. Ismail-Beigi, Modifying the electronic orbitals of nickelate heterostructures via structural distortions, *Phys. Rev. Lett.* **110**, 186402 (2013).
- [21] C.-H. Yee, T. Birol, and G. Kotliar, Guided design of copper oxysulfide superconductors, *EPL (Europhysics Letters)* **111**, 17002 (2015).
- [22] D. Li, B. Y. Wang, K. Lee, S. P. Harvey, M. Osada, B. H. Goodge, L. F. Kourkoutis, and H. Y. Hwang, Superconducting Dome in  $\text{Nd}_{1-x}\text{Sr}_x\text{NiO}_2$  Infinite Layer Films, *Phys. Rev. Lett.* **125**, 027001 (2020).
- [23] D. Li, K. Lee, B. Y. Wang, M. Osada, S. Crossley, H. R. Lee, Y. Cui, Y. Hikita, and H. Y. Hwang, Superconductivity in an infinite-layer nickelate, *Nature* **572**, 624 (2019).
- [24] M. Osada, B. Y. Wang, K. Lee, D. Li, and H. Y. Hwang, Phase diagram of infinite layer praseodymium nickelate  $\text{Pr}_{1-x}\text{Sr}_x\text{NiO}_2$  thin films, *Phys. Rev. Materials* **4**, 121801 (2020).
- [25] A. Botana, F. Bernardini, and A. Cano, There's plenty of room at the bottom, *J. Exp. Theor. Phys.* **132**, 618 (2020).
- [26] A. S. Botana and M. R. Norman, Similarities and Differences between  $\text{LaNiO}_2$  and  $\text{CaCuO}_2$  and Implications for Superconductivity, *Phys. Rev. X* **10**, 011024 (2020).
- [27] F. Bernardini, A. Bosin, and A. Cano, Geometric effects in the infinite-layer nickelates, *Phys. Rev. Materials* **6**, 044807 (2022).
- [28] B. H. Goodge, B. Geisler, K. Lee, M. Osada, B. Y. Wang, D. Li, H. Y. Hwang, R. Pentcheva, and L. F. Kourkoutis, Resolving the polar interface of infinite-layer nickelate thin films, *Nature Materials* (2023).
- [29] M. A. Hayward and M. J. Rosseinsky, Synthesis of the infinite layer Ni(I) phase  $\text{NdNiO}_{2+x}$  by low temperature reduction of  $\text{NdNiO}_3$  with sodium hydride, *Solid State Sci.* **5**, 839 (2003).
- [30] A. Schilling, M. Cantoni, J. D. Guo, and H. R. Ott, Superconductivity above 130 K in the Hg–Ba–Ca–Cu–O system, *Nature* **363**, 56 (1993).
- [31] S. Zeng, C. S. Tang, X. Yin, C. Li, M. Li, Z. Huang, J. Hu, W. Liu, G. J. Omar, H. Jani, Z. S. Lim, K. Han, D. Wan, P. Yang, S. J. Pennycook, A. T. S. Wee, and A. Ariando, Phase Diagram and Superconducting Dome of Infinite-Layer  $\text{Nd}_{1-x}\text{Sr}_x\text{NiO}_2$  Thin Films, *Phys. Rev. Lett.* **125**, 147003 (2020).
- [32] M. Osada, B. Y. Wang, B. H. Goodge, K. L. H. Yoon, K. Sakuma, D. Li, M. Miura, L. F. Kourkoutis, and H. Y. Hwang, A Superconducting Praseodymium Nickelate with Infinite Layer Structure, *Nano Lett.* **20**, 5735 (2020).
- [33] X. Ding, C. C. Tam, X. Sui, Y. Zhao, M. Xu, J. Choi, H. Leng, J. Zhang, M. Wu, H. Xiao, X. Zu, M. Garcia-Fernandez, S. Agrestini, X. Wu, Q. Wang, P. Gao, S. Li, B. Huang, K.-J. Zhou, and L. Qiao, Critical role of hydrogen for superconductivity in nickelates, *Nature* **615**, 50 (2023).
- [34] N. Kitamine, M. Ochi, and K. Kuroki, Designing nickelate superconductors with  $d^8$  configuration exploiting mixed-anion strategy, *Phys. Rev. Res.* **2**, 042032 (2020), [arXiv:2007.01153](https://arxiv.org/abs/2007.01153).
- [35] M. Hirayama, T. Tadano, Y. Nomura, and R. Arita, Materials design of dynamically stable d9 layered nickelates, *Phys. Rev. B* **101**, 1 (2020), [arXiv:1910.03974](https://arxiv.org/abs/1910.03974).
- [36] F. Bernardini, A. Demourgues, and A. Cano, Single-layer T'-type nickelates:  $\text{Ni}^{1+}$  is  $\text{Ni}^{1+}$ , *Phys. Rev. Materials* **5**, L061801 (2021).
- [37] Y. Tsujimoto, J. Sugiyama, M. Ochi, K. Kuroki, P. Manuel, D. D. Khalyavin, I. Umegaki, M. Månsson, D. Andreica, S. Hara, T. Sakurai, S. Okubo, H. Ohta, A. T. Boothroyd, and K. Yamaura, Impact of mixed anion ordered state on the magnetic ground states of  $S = 1/2$  square-lattice quantum spin antiferromagnets,  $\text{Sr}_2\text{NiO}_3\text{Cl}$  and  $\text{Sr}_2\text{NiO}_3\text{F}$ , *Phys. Rev. Mater.* **6**, 114404 (2022).
- [38] J. Zhang, A. S. Botana, J. W. Freeland, D. Phelan, H. Zheng, V. Pardo, M. R. Norman, and J. F. Mitchell, Large orbital polarization in a metallic square-planar nickelate, *Nat. Phys.* **13**, 864 (2017).
- [39] G. A. Pan, D. F. Segedin, H. LaBollita, Q. Song, E. M. Nica, B. H. Goodge, A. T. Pierce, S. Doyle, S. Novakov, D. C. Carrizales, A. T. N'Diaye, P. Shafer, H. Paik, J. T. Heron, J. A. Mason, A. Yacoby, L. F. Kourkoutis, O. Erten, C. M. Brooks, A. S. Botana, and J. A. Mundy, Superconductivity in a quintuple-layer square-planar nickelate, *Nature Materials* **21**, 160 (2021).
- [40] W. B. Jensen, Chapter II - Crystal Coordination Formulas: A flexible notation for the interpretation of solid-state structures, in *The Structures of Binary Compounds*, Cohesion and Structure, Vol. 2, edited by J. Hafner, F. Hulliger, W. Jensen, J. Majewski, K. Mathis, P. Villars, and P. Vogl (North-Holland, 1989) pp. 105–146.
- [41] J. K. Harada, K. R. Poeppelmeier, and J. M. Rondinelli, Predicting the structure stability of layered heteroanionic materials exhibiting anion order, *Inorganic Chemistry* **58**, 13229 (2019).
- [42] See Supplemental Material at [URL will be inserted by publisher] for additional computational details, electronic structure analysis, magnetic interactions, and synthesis reactions.
- [43] K. Wissel, F. Bernardini, H. Oh, S. Vasala, R. Schoch, B. Blaschkowski, P. Glatzel, M. Bauer, O. Clemens, and

- A. Cano, Single-Layer T' Nickelates: Synthesis of the La and Pr Members and Electronic Properties across the Rare-Earth Series, *Chemistry of Materials* **34**, 7201 (2022).
- [44] Y. Tsujimoto, K. Yamaura, and E. Takayama-Muromachi, Oxyfluoride chemistry of layered perovskite compounds, *Applied Sciences* **2**, 206 (2012).
- [45] A. M. Glazer, The classification of tilted octahedra in perovskites, *Acta Crystallographica Section B* **28**, 3384 (1972).
- [46] J. A. Slezak, J. Lee, M. Wang, K. McElroy, K. Fujita, B. M. Andersen, P. J. Hirschfeld, H. Eisaki, S. Uchida, and J. C. Davis, Imaging the impact on cuprate superconductivity of varying the interatomic distances within individual crystal unit cells, *Proceedings of the National Academy of Sciences* **105**, 3203 (2008).
- [47] E. Pavarini, I. Dasgupta, T. Saha-Dasgupta, O. Jepsen, and O. K. Andersen, Band-Structure Trend in Hole-Doped Cuprates and Correlation with  $T_{cmax}$ , *Phys. Rev. Lett.* **87**, 047003 (2001).
- [48] L. F. Feiner, M. Grilli, and C. Di Castro, Apical oxygen ions and the electronic structure of the high- $T_c$  cuprates, *Phys. Rev. B* **45**, 10647 (1992).
- [49] V. I. Voronin, A. E. Teplykh, and B. N. Goshchitskii, Neutron diffraction study of anisotropy of crystal lattice compression in irradiated of fast neutron high- $T_c$  superconductors  $YBa_2Cu_3O_{6.95}$  and  $La_{1.83}Sr_{0.17}CuO_4$  under pressure, *High Pressure Research* **17**, 209 (2000).
- [50] E. V. Antipov, A. M. Abakumov, and S. N. Putilin, Chemistry and structure of hg-based superconducting cu mixed oxides, *Superconductor Science and Technology* **15**, R31 (2002).
- [51] K. Wissel, A. M. Malik, S. Vasala, S. Plana-Ruiz, U. Kolb, P. R. Slater, I. da Silva, L. Alff, J. Rohrer, and O. Clemens, Topochemical Reduction of  $La_2NiO_3F_2$ : The First Ni-Based Ruddlesden-Popper  $n=1$  T'-Type Structure and the Impact of Reduction on Magnetic Ordering, *Chem. Mater.* **32**, 3160 (2020).
- [52] A. Miura, C. J. Bartel, Y. Goto, Y. Mizuguchi, C. Moriyoshi, Y. Kuroiwa, Y. Wang, T. Yaguchi, M. Shirai, M. Nagao, N. C. Rosero-Navarro, K. Tadanaga, G. Ceder, and W. Sun, Observing and modeling the sequential pairwise reactions that drive solid-state ceramic synthesis, *Advanced Materials* **33**, 2100312 (2021).
- [53] K. B. Chang, A. Vinokur, R. A. F. Pnlac, M. R. Suchomel, M. R. Marvel, and K. R. Poeppelmeier, How lewis acidity of the cationic framework affects  $KNaNbOF_5$  polymorphism, *Inorg. Chem.* **53**, 6979 (2014).
- [54] L. N. Walters, C. Zhang, V. P. Dravid, K. R. Poeppelmeier, and J. M. Rondinelli, First-Principles Hydrothermal Synthesis Design to Optimize Conditions and Increase the Yield of Quaternary Heteroanionic Oxychalcogenides, *Chem. Mater.* **33**, 2726 (2021).
- [55] F. Karsai, M. Humer, E. Flage-Larsen, P. Blaha, and G. Kresse, Effects of electron-phonon coupling on absorption spectrum:  $k$  edge of hexagonal boron nitride, *Phys. Rev. B* **98**, 235205 (2018).
- [56] M. Hepting, D. Li, C. J. Jia, H. Lu, E. Paris, Y. Tseng, X. Feng, M. Osada, E. Been, Y. Hikita, Y. D. Chuang, Z. Hussain, K. J. Zhou, A. Nag, M. Garcia-Fernandez, M. Rossi, H. Y. Huang, D. J. Huang, Z. X. Shen, T. Schmitt, H. Y. Hwang, B. Moritz, J. Zaanen, T. P. Devereaux, and W. S. Lee, Electronic structure of the parent compound of superconducting infinite-layer nickelates, *Nat. Mater.* **19**, 381 (2020).
- [57] K.-W. Lee and W. E. Pickett, Infinite-layer  $LaNiO_2$ :  $Ni^{1+}$  is not  $Cu^{2+}$ , *Phys. Rev. B* **70**, 165109 (2004).
- [58] F. C. Zhang and T. M. Rice, Effective hamiltonian for the superconducting cu oxides, *Phys. Rev. B* **37**, 3759 (1988).
- [59] L. Braicovich, L. J. P. Ament, V. Bisogni, F. Forte, C. Aruta, G. Balestrino, N. B. Brookes, G. M. De Luca, P. G. Medaglia, F. M. Granozio, M. Radovic, M. Salluzzo, J. van den Brink, and G. Ghiringhelli, Dispersion of Magnetic Excitations in the Cuprate  $La_2CuO_4$  and  $CaCuO_2$  Compounds Measured Using Resonant X-Ray Scattering, *Phys. Rev. Lett.* **102**, 167401 (2009).
- [60] P. A. Lee, N. Nagaosa, and X.-G. Wen, Doping a mott insulator: Physics of high-temperature superconductivity, *Rev. Mod. Phys.* **78**, 17 (2006).
- [61] W. E. Pickett, Spin-density-functional-based search for half-metallic antiferromagnets, *Physical Review B* **57**, 10613 (1998).
- [62] A. Gourgout, G. Grissonnanche, F. Laliberté, A. Ataei, L. Chen, S. Verret, J.-S. Zhou, J. Mravlje, A. Georges, N. Doiron-Leyraud, and L. Taillefer, Seebeck coefficient in a cuprate superconductor: Particle-hole asymmetry in the strange metal phase and fermi surface transformation in the pseudogap phase, *Phys. Rev. X* **12**, 011037 (2022).
- [63] N. Doiron-Leyraud, C. Proust, D. LeBoeuf, J. Levallois, J.-B. Bonnemaison, R. Liang, D. A. Bonn, W. N. Hardy, and L. Taillefer, Quantum oscillations and the fermi surface in an underdoped high- $t_c$  superconductor, *Nature* **447**, 565 (2007).
- [64] X. Ding, C. C. Tam, X. Sui, Y. Zhao, M. Xu, J. Choi, H. Leng, M. W. Ji Zhang, H. Xiao, X. Zu, M. Garcia-Fernandez, S. Agrestini, X. Wu, Q. Wang, P. Gao, S. Li, B. Huang, K.-J. Zhou, and L. Qiao, Critical role of hydrogen for superconductivity in nickelates, *Nature* **615**, 50 (2023).
- [65] J. Goodenough and A. Manthiram, Crystal chemistry and superconductivity of the copper oxides, *Journal of Solid State Chemistry* **88**, 115 (1990).
- [66] A. C. Walters, T. G. Perring, J.-S. Caux, A. T. Savici, G. D. Gu, C.-C. Lee, W. Ku, and I. A. Zaliznyak, Effect of covalent bonding on magnetism and the missing neutron intensity in copper oxide compounds, *Nature Physics* **5**, 867 (2009).
- [67] P. V. Balachandran, A. Cammarata, B. B. Nelson-Cheeseman, A. Bhattacharya, and J. M. Rondinelli, Inductive crystal field control in layered metal oxides with correlated electrons, *APL Materials* **2**, 076110 (2014).
- [68] T. Egami and S. Billinge, Lattice Effects in High- $T_c$  Superconductors, in *Physical Properties of High Temperature Superconductors V*, edited by D. M. Ginsberg (World Scientific, Singapore, 1996) Chap. 5, pp. 267–375.
- [69] M. Jiang, M. Berciu, and G. A. Sawatzky, Critical nature of the ni spin state in doped  $ndnio_2$ , *Phys. Rev. Lett.* **124**, 207004 (2020).
- [70] N. Charles and J. M. Rondinelli, Assessing exchange-correlation functional performance for structure and property predictions of oxyfluoride compounds from first principles, *Phys. Rev. B* **94**, 174108 (2016).
- [71] R. A. Ortiz, H. Menke, F. Misják, D. T. Mantadakis, K. Fürsich, E. Schierle, G. Logvenov, U. Kaiser, B. Keimer, P. Hansmann, and E. Benckiser, Superlattice approach to doping infinite-layer nickelates, *Phys. Rev. B* **104**, 165137 (2021).

- [72] B. H. Goodge, B. Geisler, K. Lee, M. Osada, B. Y. Wang, D. Li, H. Y. Hwang, R. Pentcheva, and L. F. Kourkoutis, Resolving the polar interface of infinite-layer nickelate thin films, *Nature Materials* [10.1038/s41563-023-01510-7](https://doi.org/10.1038/s41563-023-01510-7) (2023).
- [73] Y. Tsujimoto, K. Yamaura, and E. Takayama-Muromachi, Oxyfluoride Chemistry of Layered Perovskite Compounds, *Appl. Sci.* **2**, 206 (2012).
- [74] Y. Kobayashi, Y. Tsujimoto, and H. Kageyama, Property Engineering in Perovskites via Modification of Anion Chemistry, *Annu. Rev. Mater. Res.* **48**, 303 (2018).
- [75] J. K. Harada, N. Charles, K. R. Poeppelmeier, and J. M. Rondinelli, Heteroanionic materials by design: Progress toward targeted properties, *Advanced Materials* **31**, 1805295 (2019).
- [76] H. Kageyama, K. Hayashi, K. Maeda, J. P. Attfield, Z. Hiroi, J. M. Rondinelli, and K. R. Poeppelmeier, Expanding frontiers in materials chemistry and physics with multiple anions, *Nature Communications* **9**, 1 (2018).